K. Trzebiatowski, J. Fromme, D. Duraj, L. Kulas and K. Nyka, "A Dual-Polarized 39 GHz 4x4 Microstrip Antenna Array for 5G MU-MIMO Airflight Cabin Connectivity," 2022 24th International Microwave and Radar Conference (MIKON), Gdansk, Poland, 2022, pp. 1-4, doi: 10.23919/MIKON54314.2022.9924929.

A Dual-Polarized 39 GHz 4x4 Microstrip Antenna Array for 5G MU-MIMO Airflight Cabin Connectivity

K. Trzebiatowski[1], J. Fromme[2], D. Duraj[3], L. Kulas[4], *Senior Member, IEEE*, and K. Nyka[5], *Senior Member, IEEE*
[1,3,4,5]*Department of Microwave and Antenna Engineering*,
Faculty of Electronics, Telecommunications and Informatics, Gdansk University of Technology
Gdańsk, Poland
[2] *National Instruments (NI) Dresden GmbH*
Dresden, Germany
[1] kamil.trzebiatowski@pg.edu.pl, [2] jan.fromme@ni.com, [3] damian.duraj@pg.edu.pl, [4] lukasz.kulas@pg.edu.pl, [5] krzysztof.nyka@pg.edu.pl

***Abstract*—This paper presents the design, fabrication, and experimental validation of a 39 GHz dual-polarized 4x4 microstrip antenna array. The array consists of 16 slot coupled circular microstrip patches, fed through SMPS connectors. The procedure requiring a reduced number of cables for measurement of the uniformly excited antenna array is also presented. The array exhibits 18 dBi peak gain and 2.9 GHz reflection bandwidth and is intended for use in a 5G base station inside an airplane. The presented antenna is characterized by a simple feeding system which results in a reduced number of via-holes and dielectric layers.**

***Keywords*— antenna array, dual-polarization, microstrip antenna, 5G, MU-MIMO, superposition.**

I. Introduction

The current standard in avionics for realizing sensor networks and in-flight infotainment services is to employ wired connectivity which provides reliable and high-throughput connections at the cost of high weight and complex cable routing. The emerging trend is to solve these problems by replacing wired connections with wireless networks [1-5]. Wireless connectivity reduces the required number of wires and cables which can lead to a significant decrease in connections' weight, cost, and complexity. 5G technology is especially suited for this task, as it can provide secure and reliable communication between sensor nodes and fast transmission of data for infotainment systems.

Simultaneous transmission between several nodes in a network can be realized by employing Multi-User MIMO (MU-MIMO) technique. It also allows for increasing channel capacity by exploiting multipath propagation between individual antennas. The performance of the MIMO system can be further enhanced by employing polarization diversity, where receiving and transmitting antennas can be cross-polarized. The design of a MIMO array should be suitable to accommodate this [6-8].

Several designs of dual-polarized arrays working in the millimeter-wave band can be found in the literature [9-13]. [10] shows 8x8 crossed slot microstrip radiator array integrated with four transceiver integrated circuits (ICs).

This paper is a result of the BEYOND5 (www.beyond5.eu) project which has received funding from the ECSEL Joint Undertaking (JU) under grant agreement No 876124. The JU receives support from the European Union's Horizon 2020 research and innovation programme and France, Germany, Turkey, Sweden, Belgium, Poland, Netherland, Israel, Switzerland, and Romania. The document reflects only the authors' view and the Commission is not responsible for any use that may be made of the information it contains.

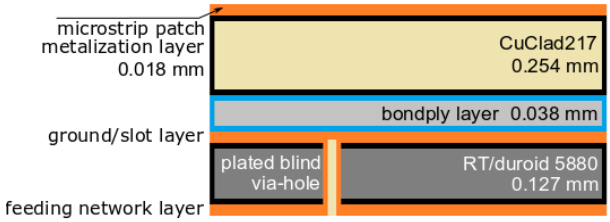

Fig. 1. Antenna stack-up design.

[11] presents 4x4 and 8x8 arrays of truncated corner stacked patch antennas driven by RFICs. In [12] four 8x8 arrays are arranged side-by-side to form a large 16x16 array. [13] shows a 4x4 array with reduced coupling between patches excited via mini-SMP connectors. The investigated designs are usually of big size and are not designed particularly for MIMO applications. They are also characterized by complex stack-ups with multiple layers and a large number of via holes.

The aim of this work is to present a compact 4x4 dual-polarized microstrip antenna array, with simplified stack-up, working in the 39 GHz frequency band and designed for a 5G network inside an airplane. The antenna array is manufactured in PCB technology and measured in a millimeter-wave anechoic chamber. The array together with a custom Radio Frequency Integrated Circuit (RFIC) will form a highly integrated antenna array system (AAS) that will be used in a 5G MU-MIMO base station.

II. Array Design

The antenna elements are designed to be fabricated in a multilayer PCB technology, with the stack-up presented in Fig. 1. Only two dielectric layers are used. The radiating patch is placed on a 0.254 mm CuClad217 substrate with a relative permittivity of 2.17 and a loss tangent of 0.002. The feeding network is designed on a 0.127 mm RT/duroid 5880 substrate (ε_r = 2.20, tgδ = 0.001). The layers are joined with a 0.038 mm bondply material (CuClad6700, ε_r = 2.35, tgδ = 0.003).

A. Antenna design

A circular microstrip patch of diameter *D* is chosen as a radiating element due to its symmetrical shape required for dual-polarized operation [14, 15]. The patch, as shown in Fig. 2, is fed through two orthogonal C-shaped slots in the ground plane. The slots are defined by three parameters: width *Ws,* lengths *Ls1, Ls2* and are placed at a distance *S1* from the patch center. The antenna is fed through miniature SMPS connectors [16] soldered to feeding microstrip lines on the bottom

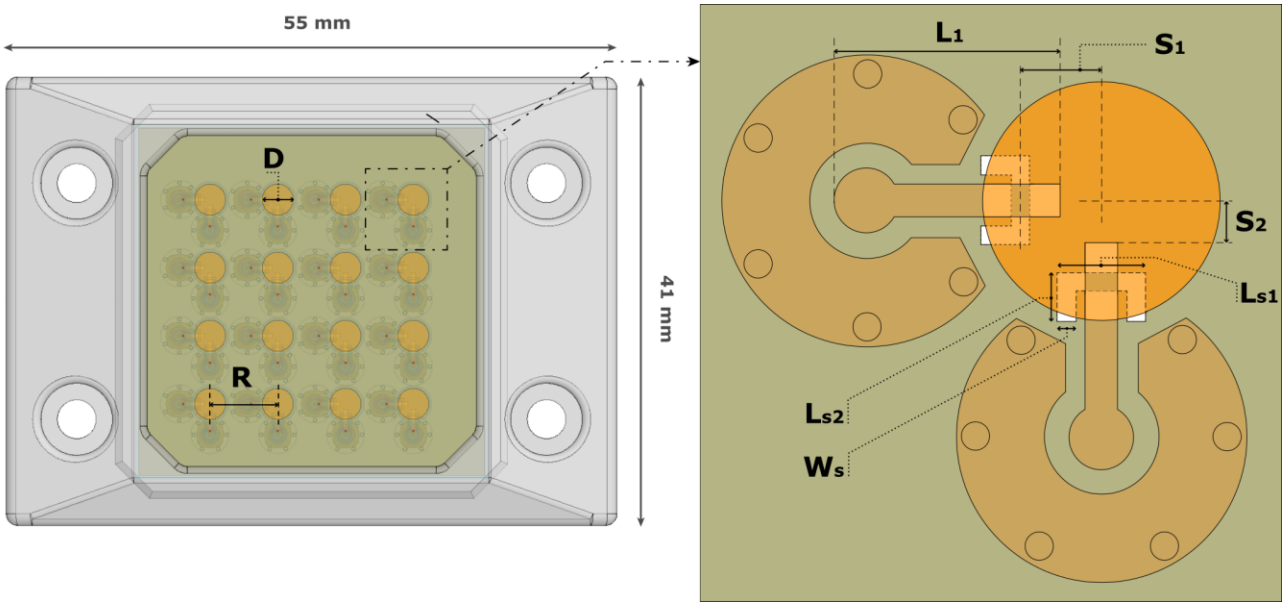

Fig. 2. Design of a dual-polarized antenna array with solder pads for SMPS connectors (top view, transparent).

TABLE I. DIMENSIONS OF THE ANTENNA ELEMENT (IN MM)

D	Ws	Ls1	Ls2	S1	S2	L1	R
2.6	0.2	0.974	0.535	0.9	0.45	2.15	5.77

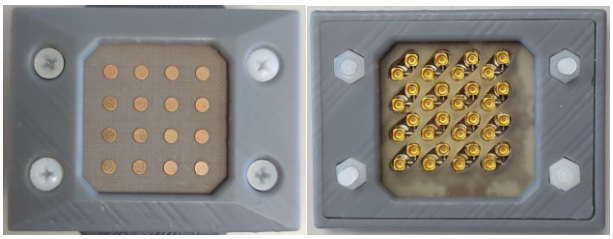

Fig. 3. Top and bottom view of the proposed antenna with 3D printed casing reinforcing SMPS connector array (2x4x4).

layer. They have a length of *Ls1* and are placed with an offset of *S2* from the patch center. The numerical values of the dimensions are presented in Table I.

The array elements are placed with a spacing *R* between them, which is constrained by connector size and a diameter of a single patch. The R value was chosen as $0.75\lambda_0$, where λ_0 is the free space wavelength at the resonance frequency (39 GHz). The array is formed by 16 elements, each consisting of radiating patch and feeding network and it is encased in a 3-D printed package, as seen in Fig. 3. A single patch can be excited with horizontal (H) or vertical (V) polarization.

B. *Numerical simulations*

The simulations were performed to optimize the antenna dimensions. They were carried out in Altair Feko 2021 environment. The goal was to maintain acceptable isolation (less than -20 dB) between all ports and cross-polarization level with proper matching (e. g. |S11| < -15 dB) for all 32 antenna ports. The array was optimized by sweeping the dimensions presented in Table I. The simulation results are presented in Figures 4 – 6 and compared with measurements of the realized prototype. The measured |S11| < -10 dB matching band is

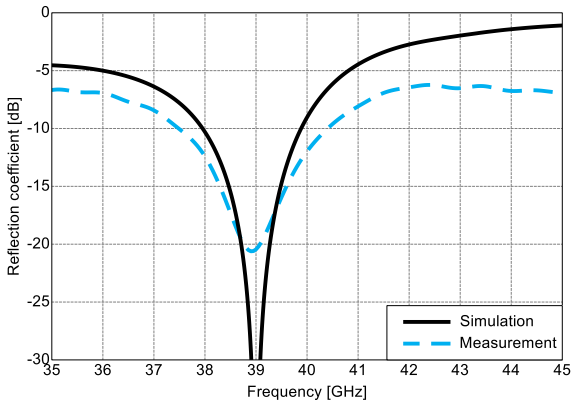

Fig. 4. Reflection coefficient of a single antenna port.

37.5 GHz – 40.4 GHz and is a bit wider than the simulated 38 – 40 GHz. The isolation between two cross-polarized ports of the same antenna element is shown in Fig. 5. The simulated and measured values are very similar to each other, with the isolation value at 39 GHz exceeding 30 dB. Fig 6. presents isolation between co-polarized ports of a few chosen antenna elements. The simulated and measured values match each other very well. In the worst-case scenario of adjacent elements, the isolation is greater than 22 dB. The realized coupling values should allow for proper calibration of the MIMO system, as demonstrated in [17], where an array with similar element-to-element coupling values was used.

III. MEASUREMENTS

The antenna array was characterized under far-field conditions with the NI mmWave OTA Validation reference solution [18] which combines a high-isolation RF anechoic chamber with the mmWave Vector Signal Transceiver (VST) that serves as a high-bandwidth waveform generator and analyzer. S-Parameter measurements have been carried out by replacing the mmWave VST with a two-port Vector Network Analyzer. The instrumentation is tightly synchronized with the AUT positioner inside the anechoic chamber to produce measurement results that correspond to exact coordinates in

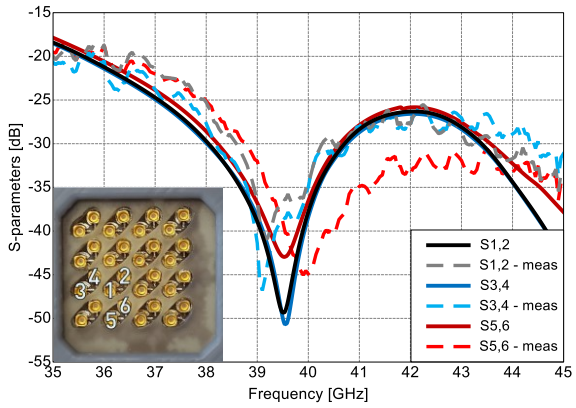

Fig. 5. Isolation between single element cross-polarized ports (simulated and measured – *meas*).

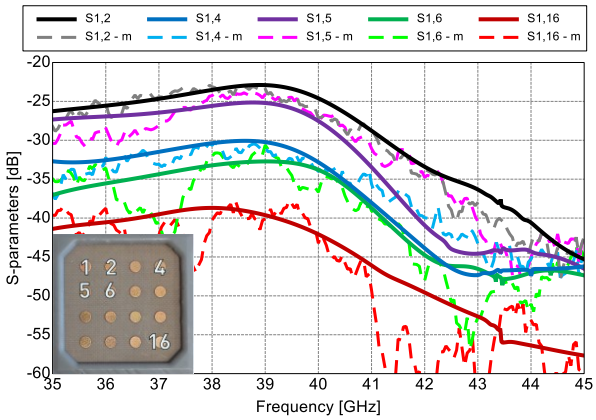

Fig. 6. Isolation between chosen co-polarized ports (simulated and measured – *m*).

space. The positioning system can rotate 360° both in azimuth and elevation direction to capture the complete radiation coming from the AUT. The measurement setup is shown in Fig 7. As a measurement probe, a dual-polarized, broadband horn antenna has been used which has 12 dBi of antenna gain at a frequency of 39 GHz (RFSpin, QRH50) [19]. The transmission coefficient (S21) has been measured for one radiating element at a time over a range of +/- 90° in azimuth (A) and elevation (E) direction with a spatial resolution of 1°.

In general, two distinct measurement procedures could be employed. In the first one (Active Element Pattern method [20]) the center and rotation axis of the AUT are fixed during the measurement process. In the second one, the AUT is repositioned during the process such that the element that is being measured is in the rotation axis of the positioning system and aligned with the center of the probe antenna's beam.

The first method (AEP) allows for the measurement of phase relations between all antenna elements and is faster to carry out as the AUT does not need to be repositioned. Furthermore, it enables the evaluation of the performance of the complete array via the application of the superposition principle (see below) and therefore has been selected as the method of choice for this measurement campaign. The second method should provide a very accurate characterization of a single element's amplitude and phase response which was beyond scope of this paper.

For validation purposes, the radiation pattern of the uniformly excited full antenna array is calculated from the measured individual patterns via superposition. For that, at each

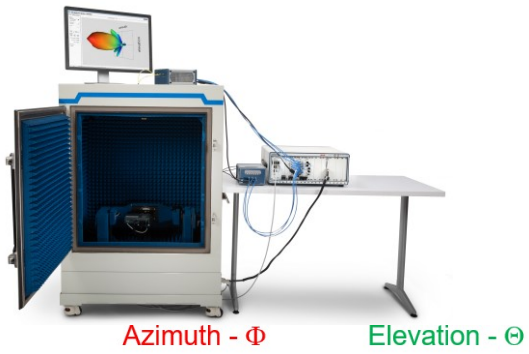

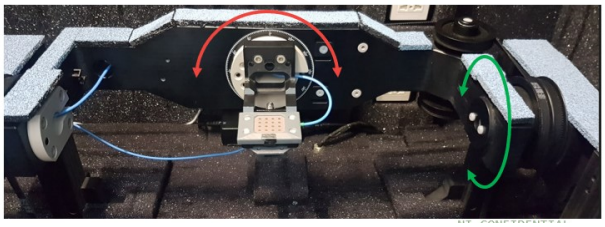

Fig. 7. NI mmWave OTA Validation Reference Solution.

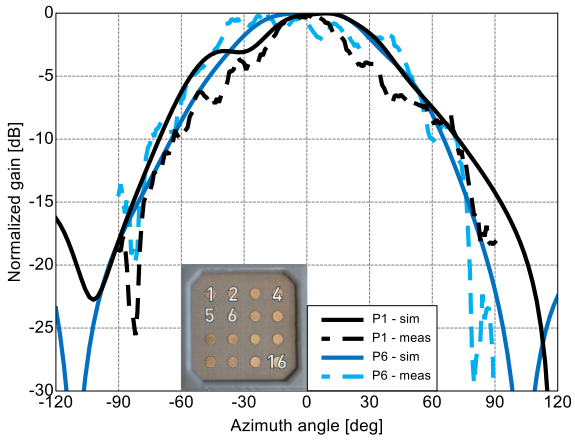

Fig. 8. Single element radiation patterns (for elements 1 and 6), (simulated and measured - *meas*).

spatial position, the measured complex transmission coefficients of each antenna patch are summed up (Eq. 1), where E is the electric field in the far-field region

$$\vec{E}(\theta,\phi)_{full\ array} = \sum_{i=1}^{N} \vec{E_i}(\theta,\phi)_{single\ element} \quad (1)$$

To validate the simulated performance of the array, the measured and simulated radiation patterns of every single radiating element have been compared. Additionally, the superposition of the measured radiation patterns, the superposition of simulated radiation patterns of 16 single antenna elements (*sum*), and the simulation of a full uniformly excited 4 x 4 antenna array (*full4x4*) have been compared.

As an example, the measurements and simulations of two single patches are depicted in Fig 8. It can be observed that the measured results do match well with the simulated pattern. The results of the superposition can be seen in Fig. 9 and Fig. 10. Again, a good correlation between the measurements and the simulations can be seen. The main beam and sidelobes are well-formed and the location of the sidelobes and nulls are very symmetric as expected.

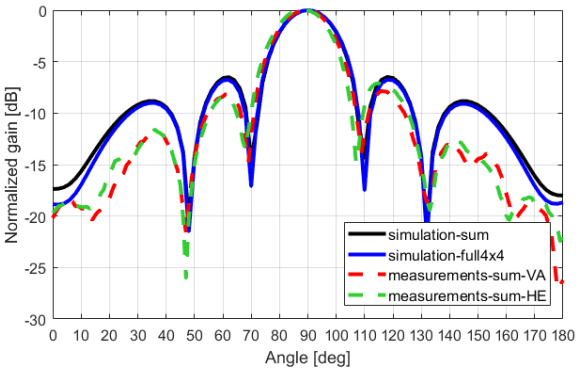

Fig. 9. Superposition results for vertical polarization (azimuth cut, VA) and horizontal polarization (elevation cut, HE) at 39 GHz.

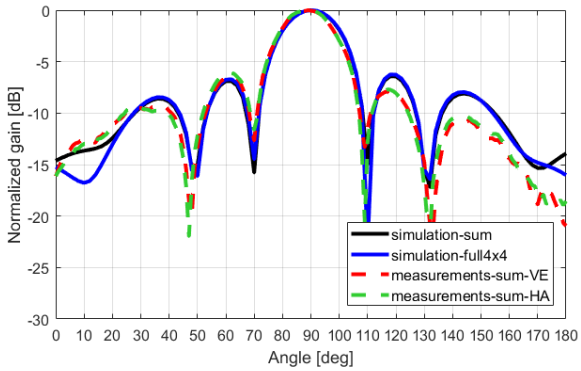

Fig. 10. Superposition results for vertical polarization (elevation cut, VE) and horizontal polarization (azimuth cut, HA) at 39 GHz.

The simulated gain for a single element is in the range of 6 – 7.5 dBi depending on the antenna element, and the gain of the uniformly excited array is about 18 dBi. Measurements of the gain were not performed due to the lack of a gain reference antenna.

IV. Conclusion

In this work, we presented a dual-polarized antenna array with 16 radiating elements designed to work in a 39 GHz 5G MU-MIMO network. The antenna is suitable for MIMO system calibration and can be employed in an airflight cabin connectivity scenario.

We also presented how the elementary radiation patterns can be added allowing for simple sequential measurement (with a limited number of simultaneous cable connections) of the radiation pattern of a uniformly excited array with a large number of elements.

The next stage of the work is to prepare the array for integration with custom transceivers. The connector array will be replaced by a BGA interface allowing for low-profile interconnection between the antenna board and the transceiver board.

References

[1] W. H. Zheng and J. T. Armstrong, “Wireless intra-spacecraft communication: the benefits and the challenges,” in *Proc. NASA/ESA Conf. Adaptive Hardware Syst.*, pp. 75–78, Jun. 2010.

[2] K. McHugh, Jr., W. Akpedeye, T. Hayajneh, “Next generation wireless-LAN: security issues and performance analysis,” in *Proc. IEEE 7th Ann. Comput. Commun. Workshop and Conf. (CCWC)*, Jan. 2017.

[3] A. Baltaci, S. Zoppi, W. Kellerer, and D. Schupke, “Evaluation of cellular IoT for energy-constrained WAIC applications,” in *Proc. IEEE 2nd 5G World Forum (5GWF)*, Oct. 2019.

[4] P. Reji et al., “Wireless intra-aircraft communication system,” in *Proc. Int. Conf. Comput. Commun. Informat. (ICCCI)*, Jan. 2020.

[5] X. Ma et al., “Multi-beam conformal patch antenna array for WAIC system application,” in *Proc. Int. Conf. Microw. Millim. Wave Techn. (ICMMT),* May 2021.

[6] P. Kyritsi, D. C. Cox, R. A. Valenzuela and P. W. Wolniansky, "Effect of antenna polarization on the capacity of a multiple element system in an indoor environment," in *IEEE J. Sel. Areas Commun.,* vol. 20, no. 6, pp. 1227-1239, Aug. 2002.

[7] J. W. Wallace, M. A. Jensen, A. L. Swindlehurst and B. D. Jeffs, "Experimental characterization of the MIMO wireless channel: data acquisition and analysis," in *IEEE Trans. Wirel. Commun.,* vol. 2, no. 2, pp. 335-343, March 2003.

[8] Liang Dong, Hosung Choo, R. W. Heath and Hao Ling, "Simulation of MIMO channel capacity with antenna polarization diversity," in *IEEE Trans. Wirel. Commun.*, vol. 4, no. 4, pp. 1869-1873, July 2005.

[9] X. Gu, D. Liu and B. Sadhu, "Packaging and antenna integration for silicon-based millimeter-wave phased arrays: 5G and Beyond," in *IEEE J. Microw.*, vol. 1, no. 1, pp. 123-134, Jan. 2021.

[10] X. Gu et al., "Development, implementation, and characterization of a 64-element dual-polarized phased-array antenna module for 28-GHz high-speed data communications," in *IEEE Trans. Microw. Theory Techn.*, vol. 67, no. 7, pp. 2975-2984, July 2019.

[11] J. -C. S. Chieh et al., "Development of flat panel active phased array antennas using 5G silicon RFICs at Ku- and Ka-bands," in *IEEE Access*, vol. 8, pp. 192669-192681, 2020.

[12] M. W. Rousstia et al., "28-GHz wideband dual-polarized parasitic-patch antenna array on tile-scale package," in *Proc. 50th Eur. Microw. Conf. (EuMC),* 2021, pp. 360-363.

[13] W. Kim, J. Bang and J. Choi, "A cost-effective antenna-in-package design with a 4 × 4 dual-polarized high isolation patch array for 5G mmWave applications," in *IEEE Access*, vol. 9, pp. 163882-163892, 2021.

[14] T. H. Jang et al., “60 GHz low-profile, wideband dual-polarized U-slot coupled patch antenna with high isolation,” in *IEEE Trans. Antennas Propag.*, vol. 67, no. 7, pp. 4459–4462, Jul. 2019.

[15] X. Yang et al., "Broadband dual-polarized phased array with broadside and endfire radiation for 5G millimeter wave communications," in *Proc. Comput., Commun. and IoT Appl. (ComComAp)*, pp. 210-212, Oct. 2019.

[16] SV Microwave, Inc., “*SMPS male PCB surface mount connector, FD”* 3811-40022-40023 datasheet, Aug. 2011 [Revised Jan. 2016].

[17] J. Vieira et al., "Reciprocity calibration for massive MIMO: proposal, modeling, and validation," in *IEEE Trans. Wirel. Commun.,* vol. 16, no. 5, pp. 3042-3056, May 2017.

[18] RFSpin website, available at: https://www.rfspin.com/

[19] NI, “*5G mmWave Over-the-Air (OTA) Validation*”, available at: https://www.ni.com/en-us/innovations/semiconductor/lab-characterization-and-validation/mmwave-ota-validation-test-reference-architecture.html

[20] D. M. Pozar, “The active element pattern,” *IEEE Trans. Antennas Propag.*, vol. 42, pp. 1176–1178, Aug. 1994